Hindawi
Computational and Mathematical Methods
Volume 2023, Article ID 5515370, 18 pages
https://doi.org/10.1155/2023/5515370

Research Article

Modeling of Angiogenesis in Tumor Blood Vessels via Lattice Boltzmann Method

Sara Zergani,[1] K. K. Viswanathan,[2,3] D. S. Sankar,[4] and P. Sambath[5]

[1]*Department of Mathematical and Physical Sciences, College of Arts and Sciences, University of Nizwa, Oman*
[2]*Department of Mathematical Modeling, Faculty of Mathematics, Samarkand State University, University Blvd., 15, Samarkand 140104, Uzbekistan*
[3]*Department of Applied Mathematics and Informatics, Termez State University, Termez City 190100, Uzbekistan*
[4]*School of Applied Sciences and Mathematics, Universiti Teknologi Brunei, Jalan Tungku Link, Gadong, BE1410, Bandar Seri Begawan, Brunei Darussalam*
[5]*Department of Mathematics, SRM Institute of Science and Technology, Kattankulathur, Tamil Nadu 603203, India*

Correspondence should be addressed to K. K. Viswanathan; visu20@yahoo.com

Received 12 February 2023; Revised 23 June 2023; Accepted 22 August 2023; Published 8 September 2023

Academic Editor: Siddhartha Chakrabarty

This mathematical model studies the dynamics of tumor growth, one of the most complex dynamics problems that relates several interrelated processes over multiple ranges of spatial and temporal scales. In order to construct a tumor growth model, an angiogenesis model is used with focus on controlling the tumor volume, preventing new establishment, dissemination, and growth. The lattice Boltzmann method (LBM) is effectively applied to Navier-Stokes' equation for obtaining the numerical simulation of blood flow through vasculature. It is observed that the flow features are extremely sensitive to stenosis severity, even at small strains and stresses, and that a severe effect on flow patterns and wall shear stresses is noticed in the tumor blood vessels. It is noted that based on the nonlinear deformation of the blood vessel's wall, the flow rate conditions became unstable or distorted and affect the complex blood vessel's geometry and it changes the blood flow pattern. When the blood flows inside the stenotic artery, depending on the presence of moderate or severe stenosis, it can lead to insufficient blood supply to the tissues in the downstream. Consequently, the highly disturbed flow occurs in the downstream of the stenosed artery, or even plaque ruptures happen when the flow pattern becomes very irregular and complex as it transits to turbulent which cannot be described without assumptions on the geometry. The results predicted by LBM-based code surpassed the expectations, and thus, the numerical results are found to be in great accord with the relevant established results of others.

1. Introduction

During the past decades, several experimental techniques have been developed to contribute to the knowledge of tumor growth dynamics and immune system interactions [1, 2]. Theoretical, experimental, and clinical studies on tumor growth progressed significantly to advance the understanding on the development mechanism of cancer, the evolving process of tumor angiogenesis, and the migration of new blood vessels and capillaries to the tumor blood vessels. On the other hand, the mechanisms that have a function in tumor-induced angiogenesis' interactions with the avascular growth system remain unknown.

Tumor blood vessels are structurally abnormal, physically aberrant, and functionally inefficient; as a result, the tumor vascular networks are not fully perfused, and chemotherapeutics are not delivered uniformly to tumor cells. Angiogenesis is the process by which new blood vessels grow and is a critical component of wound healing, providing nutrients to newly formed tissue. This process also involves the migration, growth, and differentiation of endothelial cells, which are found inside the blood vessels' wall. It is also a mechanism to sustain tumor progression by maintaining oxygen supply to the tumor as well as to its growth and development. Tumor-induced angiogenesis also involves the process of forming new blood vessels from the existing

capillaries by endothelial cell sprouting, proliferation, and fusion; thus, it is a critical component of solid tumor growth [3].

In recent years, there have been several authors who have investigated the repercussions of blood flow via a vascular network on tumor growth [4–7] and employing cellular automaton (CA) to tumor growth models which are combined with the network models of the vasculature. These authors had given due consideration to the vascular network inhomogeneities, stress-induced blood vessel collapse, and therapeutic implications to them. Accordingly, some researchers attempted to consider the remodeling of tumor-induced angiogenesis which dates back to the work of Balding and McElwain [8] on this subject. Mantzaris et al. [9] and Chaplain et al. [10] made a seminal contribution to this research area. Some relevant subject areas such as avascular growth and angiogenesis have been quite thoroughly discussed through the mathematical modeling approach, while other topics like vascular tumor growth have received considerably less interest and attention. For instance, the scientific investigation of Orme and Chaplain [11] focused on vascular tumor growth and invasion. Zheng et al. [12] have recently enhanced and combined a level-set method for solid tumor growth with a hybrid continuous discrete angiogenesis model which was initially studied by Anderson and Chaplain [13].

This research is aimed at providing a new contribution in this direction through a mathematical model that combines tumor dynamics and interactions between a vascular growth and angiogenesis. Anderson et al. [14] along with many authors Gerlee and Anderson [15–17], Cristi et al. [18], and Schmitz et al. [19] established mathematical models to describe the characteristics of cancer dynamics, by integrating the gathered information in their model.

A wide range of mathematical models (discrete, continuous, and hybrid) have been used to model the elements of cancer progression (Duchting and Dehl [20], Duchting and Vogelsaenger [21, 22], Duchting et al. [23], and Kansal et al. [24]) as well as to make better understanding on cancer dynamics, tumor growth, and metastasis. Discrete models track and update individual cells according to a set of biological rules [25, 26]. Discrete models shall be classified as lattice-based models or lattice-free models. Lattice-based models might be further classified one of the types, such as lattice gas cellular automata model (LGCA), cellular automata (CA), and cellular Potts models (CPMs). In this connection, stochastic models and finite-difference approximation methods are acclimated into the lattice-free approaches. Even while various cellular automata approaches have revealed anomalies in the invading front of the cells (Hatzikirou and Deutsch [27]; Jiang et al. [28]), the invasion process has not been well explored.

Continuum models investigate the tumor tissue as a continuous medium and use differential equations to model it (Frieboes et al. [29] and Lowengrub et al. [30]). Ordinary differential equations (ODEs) and partial differential equations (PDEs) were employed in continuum modeling. PDEs frequently use too large scale and are ineffective when the challenge concentrates on a tiny number of individual cancer cells. Single cell-matrix interactions cause the tumor front to enter into healthy tissue which is a critical issue in the invasion. Logistic power and the Gompertz law are the basics involved in the formation of ODEs in continuum modeling. From this perspective, PDEs such as reaction-diffusion and partial integrodifferential equations are exerted.

Hybrid models are accomplished by two models [31, 32] that combine the benefits of discrete and continuous modeling and use the appropriate methodologies to represent the chemical interactions and tissue landscapes in a single model. In their investigation, hybrid models are constructed by combining discrete and continuum approaches for modeling and simulating the cell dynamics. Multitudinous tumor microenvironmental variables such as matrix-degrading enzymes, extracellular matrix (ECM), oxygen, growth factors, and inhibitors are taken into account in the formation of mathematical models.

Specific models of cancer cell invasion have been used to explain the diverse aspects of tumor growth dynamics which include discrete models (considering cells as individual entities) [19, 33], continuum models (using reaction-diffusion equations) [34–38], and hybrid models [27, 39, 40]. Moreover, these models ignore all crucial geometrical aspects, which are peculiar to continuous models, but they play an important role in real-world system evolution. In fact, in reality, these models were related to significant phenomena like angiogenesis, angiostatin effects, and metastatic detachment, which cannot be clearly understood without making use of geometric assumptions.

The mathematical representation of the tumor's progression in the presence of angiogenesis and the mathematical structure of the model are both quite difficult. The effects of blood flow through a vasculature in any arterial geometry with tumor growth and angiogenesis can be better understood using computer simulation approaches, and thus, these simulation techniques have been used in a variety of biomechanical applications ranging from blood vessels and tissue structural features to fluid dynamic phenomena like blood flow. Applied scientists have developed a highly abstract cellular automaton model of early cancer growth and a lattice model of blood-oxygen flow to study the effects of knocking out pairs of "cancer hallmarks." Many diseases are associated with the abnormal rheology of blood. More generally, the function of blood vessels and their dynamics were discussed in relation to cancer (tumor angiogenesis) and both vascular disorders that result in blood vessel anomalies like aneurysms. These abnormalities are usually produced by unhealthy red blood cells with a changed form that has trouble passing through microvessels. Unfortunately, due to challenges in distinguishing the fundamental drivers of flow in vivo or in vitro, experimental methods for these problems are limited.

These issues are overcome by computer models; however, most focus on reproducing the macroscopic, continuous feature of blood flow by making numerous simplifying assumptions. Unfortunately, these models are unable to account the link between microscopic cellular flow dynamics and macroscopic tumor tissue. The aim of the present research is to apply a suitable lattice approach that can predict various impacts of blood flow in complex microvascular

geometry, by explicitly accounting the shape of the metastatic process (tumor angiogenesis), and cancer cellular automata (CA) model. The application of the LBM to blood flow has piqued the interest of scholars in recent years [41–52]. For instance, the thrombus formation in blood flow is predicted by [50, 51, 53, 54] the blood flow simulation in the microvascular bifurcations, and according to [55–58], blood cell shape and interactions between the inflow and outflow are also taken into account. Lattice Boltzmann method (LBM) is applied to study the blood flow, and the main goal of this study is to connect the two scales: the microscopic scale of a cell and the mesoscopic scale of blood flow surrounding a tumor in order to develop a biologically relevant cancer growth model that could be employed in cancer treatment research.

Due to the recent findings along with the advantages of the applied methods, many difficult issues have been successfully addressed using the LBM including for compressible fluid flow [59]; multiphase and multicomponent fluids [60], with particulate suspensions [61] using reaction-diffusion system [62]; and flow through porous media [63, 64]. In other aspects, this method shows a variety of the flow patterns and their flow instabilities which can be applied to the number of equations of mathematical physics, including wave motion equations [65], Burgers' equations [66], KdV equation [67], and nonlinear Schrodinger equations [68]. Alemani et al. [69] coupled a 2-state cellular automata model of cancer tumor with a lattice fluid model of nutrition diffusion [60]. This simulation demonstrated that a tumor may grow from a single healthy cell in an acceptable amount of time up to a biologically consistent size, using cellular automata such as cancer cells and the lattice methods for biofluid dynamics problems. This flexible, powerful, and customizable approach can be used to predict and model a framework for the blood flow properties in multitudinous vessel geometry and with a wide range of blood composition. The LBM has a significant benefit as it can mimic particulate flow dynamics as well as in a variety of geometries.

The aim of this study is to formulate a computational model to study the tumor-induced angiogenesis with the support of mathematical framework and numerical simulation by lattice Boltzmann method (LBM). The fundamental biological processes associated with the angiogenesis are discussed, and these are incorporated into the proposed mathematical model. LBM has been proposed as a potential computational method for obtaining the numerical solution of the mathematical model that represents tumor angiogenesis which is applied to study the various effects of blood flow in microvascular networks with the complexities. To validate the formulated mathematical model and computational methodology, the obtained LBM solution is compared with the results of Pontrelli et al. [70]. To authenticate the results of this study, we compare the obtained data with the data of Sun and Munn [48], Liu [71], and Harrison [72].

2. Governing Equations

2.1. Navier-Stokes' Equation. Continuity equation and Navier-Stokes' equations are the governing equations for the calculation of the velocity field and pressure distribution in the rheology of blood under normal/abnormal state. The Navier-Stokes equations are implemented for the computational blood flow determination in models such as stenosis and hydrostatic stress by restricting the radii of the vessels.

Continuity equation:

$$\frac{\partial \rho}{\partial t} + \nabla.(\rho.u) = 0. \tag{1}$$

Momentum equations (Navier-Stokes' equations):

$$\rho\left(\frac{\partial u}{\partial t} + u\frac{\partial u}{\partial x} + v\frac{\partial u}{\partial y} + w\frac{\partial u}{\partial z}\right) = -\frac{\partial p}{\partial x} + \mu\left[\frac{\partial^2 u}{\partial x^2} + \frac{\partial^2 u}{\partial y^2} + \frac{\partial^2 u}{\partial z^2}\right] + \rho \cdot g_x, \tag{2}$$

$$\rho\left(\frac{\partial v}{\partial t} + u\frac{\partial v}{\partial x} + v\frac{\partial v}{\partial y} + w\frac{\partial v}{\partial z}\right) = -\frac{\partial p}{\partial y} + \mu\left[\frac{\partial^2 v}{\partial x^2} + \frac{\partial^2 v}{\partial y^2} + \frac{\partial^2 v}{\partial z^2}\right] + \rho \cdot g_y, \tag{3}$$

$$\rho\left(\frac{\partial w}{\partial t} + u\frac{\partial w}{\partial x} + v\frac{\partial w}{\partial y} + w\frac{\partial w}{\partial z}\right) = -\frac{\partial p}{\partial z} + \mu\left[\frac{\partial^2 w}{\partial x^2} + \frac{\partial^2 w}{\partial y^2} + \frac{\partial^2 w}{\partial z^2}\right] + \rho \cdot g_z, \tag{4}$$

where g_x, g_y, and g_z denotes the gravity along x, y, and z directions, respectively.

2.2. Lattice Boltzmann Equation. The lattice Boltzmann equation including a force term on a nine-velocity square lattice is

$$f_\alpha(X + e_\alpha \Delta t, t + \Delta t) - f_\alpha(X, t) = -\frac{1}{\tau}\left(f_\alpha - f_\alpha^{\mathrm{eq}}\right) + \frac{\Delta t}{6e^2} e_{\alpha i} F_i. \tag{5}$$

$f_\alpha(x, t)$is the particle distribution function, where$x$is the space vector and$t$is the time;$e_\alpha$is the particle velocity vector, where $\alpha = 1, \cdots, 9$; $e = \Delta x/\Delta t$, where Δx is the lattice size and $\Delta t$is the time step; and$\tau$is the single relaxation time factor. The stability of the equation requires that $\tau > (1/2)$. Based on the conditions in test cases (please refer to the part of Numerical Results and Discussion for details), the single relaxation time parameter is approximately $\tau = 1.5$, and $f_\alpha^{(\mathrm{eq})}(x, t)$ is the equilibrium distribution function at time t, x, which is the Maxwell–Boltzmann distribution function. F_i is the ith direction force component and is defined as

$$F_i = F_{pi} + F_{bi} + F_{wi} + F_{ci}, \tag{6}$$

$$F_{pi} = -gh\frac{\partial z_b}{\partial x_i}, \tag{7}$$

$$F_{bi} = C_b u_i \sqrt{u_i u_i}, \tag{8}$$

$$F_{wi} = \frac{\rho_a}{\rho_w} C_w u_{wi} \sqrt{u_{wi} u_{wi}}, \tag{9}$$

$$F_{ci} = \begin{cases} f_c h u_y, & i = x, \\ -f_c h u_x, & i = y, \end{cases} \tag{10}$$

$$F_i = -gh \frac{\partial z_b}{\partial x_i} + C_b u_i \sqrt{u_i u_i} + \frac{\rho_a}{\rho_w} C_w u_{wi} \sqrt{u_{wi} u_{wi}} + F_{ci}, \tag{11}$$

consisting of an appropriate hydrostatic pressure approximation, where F_{bi} denotes the stress of the shear wind, F_{pi} is the stress of the shear bed, and F_{wi} is the Coriolis effect forcing term, $F_{ci}.f_c = 2\omega \sin \varphi$ is the Coriolis parameter, ω is the rotation rate of the earth, φ is the latitude, z_b is the bed elevation, $C_b = g/C_z^2$ is the bed friction coefficient, and $C_z = h^{1/6}/n_b$ is both the Chezy and the Manning coefficients at the bed, n_b,$[L^{-1/3}T]$. ρ_ω gives the density, ρ_a gives the air density, $C_w = (0.63 + 0.66\sqrt{u_{wi} u_{wi}}) \times 10^{-3}$is the expression for the coefficient of the wind, and u_{wi} is the ith direction velocity of the wind.

2.3. Lattice Arrangements (D2Q9). The model is used mostly for solving the fluid flow problem. On the 9-speed square lattice shown in Figure 1, each particle moves one lattice unit at its velocity only along the eight links indicated with 1-8, in which 0 indicates the rest particle with zero speed. The particles velocity vector is defined by

$$e_\alpha = \begin{cases} (0,0), & \alpha = 0, \\ e\left[\cos \dfrac{(\alpha-1)\pi}{4}, \sin \dfrac{(\alpha-1)\pi}{4}\right], & \alpha = 1,3,5,7, \\ \sqrt{2}e\left[\cos \dfrac{(\alpha-1)\pi}{4}, \sin \dfrac{(\alpha-1)\pi}{4}\right], & \alpha = 2,4,6,8. \end{cases} \tag{12}$$

In this, the central particle speed is zero, while the velocity vectors are very high. The respective speed on elements f_0, f_1,…f_6, f_7, and f_8 is $e_0(0,0)$, $e_1(1,0)$, $e_3(0,1)$, $e_5(-1,0)$, $e_7(0,-1)$, $e_2(1,1)$, $e_4(-1,1)$, $e_6(-1,-1)$, and $e_8(1,-1)$.

The weighting factors for the corresponding distribution elements are 4/9, 1/9, 1/9, 1/9, 1/9, 1/36, 1/36, 1/36, and 1/36.

2.4. Equilibrium Distribution Function for D2Q9. The aim of using the equilibrium function in the lattice Boltzmann equation is to recover the Navier-Stokes equation. A powerful and alternative way is to assume that an equilibrium function can be expressed as a power series in macroscopic velocity as

$$f_i^{\mathrm{eq}} = A_\alpha + B_\alpha e_{\alpha i} u_i + C_\alpha e_{\alpha i} e_{\alpha j} u_i u_j + D_\alpha u_i u_j. \tag{13}$$

From the symmetry of the lattice, resulting into the equation as

$$f_\alpha^{\mathrm{eq}} = \begin{cases} \rho - \dfrac{5g\rho^2}{6e^2} - \dfrac{2\rho u_i u_i}{3e^2}, & \alpha = 0, \\ \dfrac{g\rho^2}{6e^2} + \dfrac{\rho e_{\alpha i} u_i}{3e^2} + \dfrac{\rho e_{\alpha i} e_{\alpha j} u_i u_j}{2e^4} - \dfrac{\rho u_i u_i}{6e^2}, & \alpha = 1,3,5,7, \\ \dfrac{g\rho^2}{24e^2} + \dfrac{\rho e_{\alpha i} u_i}{12e^2} + \dfrac{\rho e_{\alpha i} e_{\alpha j} u_i u_j}{8e^4} - \dfrac{\rho u_i u_i}{24e^2}, & \alpha = 2,4,6,8. \end{cases} \tag{14}$$

2.5. Definition of Macroscopic Quantity. The macroscopic fluid density $\rho(X,t)$ and velocity $u(X,t)$ are computed from the particle distributions.

The physical variable fluid density ρ is

$$\begin{aligned} \rho(X,t) &= \sum_\alpha f_\alpha(X,t) = \sum_\alpha f_\alpha^{\mathrm{eq}}(X,t), \\ \rho(X,t) u_i(X,t) &= \sum_\alpha e_{\alpha i} f_\alpha(X,t) \\ &= \sum_\alpha e_{\alpha i} f_\alpha^{\mathrm{eq}}(X,t), \\ \rho(X,t) u_i(X,t) u_j(X,t) &= \sum_\alpha e_{\alpha i} e_{\alpha j} f_\alpha(X,t) \\ &= \sum_\alpha e_{\alpha i} e_{\alpha j} f_\alpha^{\mathrm{eq}}(X,t) \\ &= \frac{1}{2} g\rho^2 \delta_{ij} + \rho u_i u_j. \end{aligned} \tag{15}$$

The macroscopic quantity velocity $u(X,t)$ is defined in terms of the distribution function as

$$u_i(X,t) = \frac{1}{\rho(X,t)} \sum_\alpha e_{\alpha i} f_\alpha(X,t). \tag{16}$$

2.6. Recovery. Performing an expansion using Chapman-Enskog on the lattice Boltzmann equation recovers the macroscopic equations. Suppose that Δt (the time t new positions of molecules) is small and is equal to ε, $(\Delta t = \varepsilon)$, then Equation (5) is expressed as

$$f_\alpha(X + e_\alpha \varepsilon, t + \varepsilon) - f_\alpha(X,t) = -\frac{1}{\tau}(f_\alpha - f_\alpha^{\mathrm{eq}}) + \frac{\varepsilon}{6e^2} e_{\alpha j} F_j, \tag{17}$$

with a Taylor expansion to the first term on the left side of Equation (17) taking time and space about point (X,t) in consideration resulting as

$$\begin{aligned} f_\alpha(X + e_\alpha \varepsilon, t + \varepsilon) - f_\alpha(X,t) &= \varepsilon \left(\frac{\partial}{\partial t} + e_{\alpha j} \frac{\partial}{\partial X_j}\right) f_\alpha \\ &+ \frac{1}{2}\varepsilon^2 \left(\frac{\partial}{\partial t} + e_{\alpha j} \frac{\partial}{\partial x_j}\right)^2 f_\alpha + O(\varepsilon^2) = \frac{1}{\tau}(f_\alpha - f_\alpha^{\mathrm{eq}}) \\ &+ \frac{\varepsilon}{6e^2} e_{\alpha j} F_j, \end{aligned} \tag{18}$$

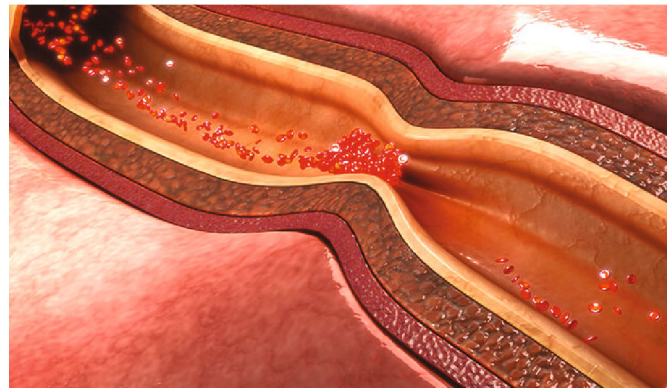

Figure 1: Tumor vessel.

where f_α around $f_\alpha^{(0)}$ can also be expanded as

$$f_\alpha = f_\alpha^{(0)} + \varepsilon f_\alpha^{(1)} + \varepsilon^2 f_\alpha^{(2)} + O(\varepsilon^2), \tag{19}$$

where $f_\alpha^{(0)} = f_\alpha^{\mathrm{eq}}$.

Expanding f_α around $f_\alpha^{(0)}$ in equation $f_\alpha = f_\alpha^{(0)} + \varepsilon f_\alpha^{(1)} + O(\varepsilon^2)$, the collision operator can be rewritten as

$$\begin{aligned} -\frac{1}{\tau}\left[\left(f_\alpha - f_\alpha^{\mathrm{eq}}\right)\right] &= -\frac{1}{\tau}\left[\left(f_\alpha^{(0)} + \varepsilon f_\alpha^{(1)} + \varepsilon^2 f_\alpha^{(2)} + O(\varepsilon^2) - f_\alpha^{\mathrm{eq}}\right)\right] \\ &= -\frac{1}{\tau}\left[\varepsilon f_\alpha^{(1)} + \varepsilon^2 f_\alpha^{(2)} + \cdots\right]. \end{aligned} \tag{20}$$

Equation (18) to order ε is

$$\begin{aligned} \varepsilon\left(\frac{\partial}{\partial t} + e_{\alpha j}\frac{\partial}{\partial X_j}\right) f_\alpha &= -\frac{1}{\tau}\varepsilon f_\alpha^{(1)} + \frac{\varepsilon}{6e^2} e_{\alpha j} F_j \longrightarrow \left(\frac{\partial}{\partial t} + e_{\alpha j}\frac{\partial}{\partial X_j}\right) f_\alpha \\ &= -\frac{1}{\tau} f_\alpha^{(1)} + \frac{1}{6e^2} e_{\alpha j} F_j \end{aligned} \tag{21}$$

and to order ε^2 is

$$\begin{aligned} &\varepsilon^2\left(\frac{\partial}{\partial t} + e_{\alpha j}\frac{\partial}{\partial X_j}\right) f_\alpha^{(1)} + \frac{1}{2}\varepsilon^2\left(\frac{\partial}{\partial t} + e_{\alpha j}\frac{\partial}{\partial X_j}\right)^2 f_\alpha^{(0)} \\ &= -\frac{1}{\tau}\varepsilon^2 f_\alpha^{(2)} \longrightarrow \left(\frac{\partial}{\partial t} + e_{\alpha j}\frac{\partial}{\partial X_j}\right) f_\alpha^{(1)} + \frac{1}{2}\left(\frac{\partial}{\partial t} + e_{\alpha j}\frac{\partial}{\partial X_j}\right)^2 f_\alpha^{(0)} \\ &= -\frac{1}{\tau} f_\alpha^{(2)} \varepsilon^2\left(\frac{\partial}{\partial t} + \mathrm{e}_{\alpha j}\frac{\partial}{\partial X_{\mathrm{j}}}\right) f_\alpha^{(1)} + \frac{1}{2}\varepsilon^2\left(\frac{\partial}{\partial t} + e_{\alpha j}\frac{\partial}{\partial X_j}\right)^2 f_\alpha^{(0)} \\ &= -\frac{1}{\tau}\varepsilon^2 f_\alpha^{(2)} \longrightarrow \left(\frac{\partial}{\partial t} + e_{\alpha j}\frac{\partial}{\partial X_{\mathrm{j}}}\right) f_\alpha^{(1)} + \frac{1}{2}\left(\frac{\partial}{\partial t} + e_{\alpha j}\frac{\partial}{\partial X_j}\right)^2 f_\alpha^{(0)} \\ &= -\frac{1}{\tau} f_\alpha^{(2)}. \end{aligned} \tag{22}$$

Substituting Equation (21) of order ε into Equation (22) of order ε^2 and after rearrangement leads to

$$\begin{aligned} \left(1 - \frac{1}{2\tau}\right)\left(\frac{\partial}{\partial t} + e_{\alpha j}\frac{\partial}{\partial x_j}\right) f_\alpha^{(1)} &= -\frac{1}{\tau} f_\alpha^{(2)} \\ &- \frac{1}{2}\left(\frac{\partial}{\partial t} + e_{\alpha j}\frac{\partial}{\partial x_j}\right)\left(\frac{1}{6e^2} e_{\alpha k} F_k\right). \end{aligned} \tag{23}$$

Taking $\sum_\alpha[(20) + \varepsilon \times (22)]$, about α provides

$$\begin{aligned} \sum_\alpha \Bigg[\left(\frac{\partial}{\partial t} + e_{\alpha j}\frac{\partial}{\partial X_j}\right) f_\alpha &= -\frac{1}{\tau} f_\alpha^{(1)} + \frac{1}{6e^2} e_{\alpha j} F_j + \varepsilon \\ &\times \left(\left(1 - \frac{1}{2\tau}\right)\left(\frac{\partial}{\partial t} + e_{\alpha j}\frac{\partial}{\partial x_j}\right) f_\alpha^{(1)} = -\frac{1}{\tau} f_\alpha^{(2)}\right. \\ &\left. - \frac{1}{2}\left(\frac{\partial}{\partial t} + e_{\alpha j}\frac{\partial}{\partial x_j}\right)\left(\frac{1}{6e^2} e_{\alpha k} F_k\right)\right] \end{aligned} \tag{24}$$

and about α gives

$$\frac{\partial}{\partial t}\left(\sum_\alpha f_\alpha^{(0)}\right) + \frac{\partial}{\partial x_j}\left(\sum_\alpha f_\alpha^{(1)}\right) = -\varepsilon \frac{1}{12e^2}\frac{\partial}{\partial x_j}\underbrace{\left(\sum_\alpha e_{\alpha j} e_{\alpha k} F_k\right)}_{0}. \tag{25}$$

By applying accuracy of the first order to the force term, local equilibrium function, and evaluating for the remaining terms in Equation (25), we obtain Equation (1) which is the continuity equation (1) for the Navier-Stokes equation.

$$\begin{aligned} \frac{\partial(\rho)}{\partial t} + \frac{\partial(\rho u_j)}{\partial x_j} &= 0, \\ \partial_t \rho + \nabla.(\rho \boldsymbol{u}) &= 0, \end{aligned} \tag{26}$$

which is the momentum equation (2) for the Navier-Stokes equation.

From $\sum_\alpha e_{\alpha i}[(20)+\varepsilon\times(22)]$, about α provides

$$\begin{aligned}\sum_\alpha e_{\alpha i}\Bigg[&\left(\left(\frac{\partial}{\partial t}+e_{\alpha j}\frac{\partial}{\partial X_j}\right)f_\alpha=-\frac{1}{\tau}f_\alpha^{(1)}+\frac{1}{6e^2}e_{\alpha j}F_j\right)\\&+\varepsilon\left(\left(1-\frac{1}{2\tau}\right)\left(\frac{\partial}{\partial t}+e_{\alpha j}\frac{\partial}{\partial x_j}\right)f_\alpha^{(1)}=-\frac{1}{\tau}f_\alpha^{(2)}\right.\\&\left.-\frac{1}{2}\left(\frac{\partial}{\partial t}+e_{\alpha j}\frac{\partial}{\partial x_j}\right)\left(\frac{1}{6e^2}e_{\alpha k}F_k\right)\right)\Bigg]\sum_\alpha e_{\alpha i}\\&\cdot\Bigg[\left(\left(\frac{\partial}{\partial t}+e_{\alpha j}\frac{\partial}{\partial X_j}\right)f_\alpha=-\frac{1}{\tau}f_\alpha^{(1)}+\frac{1}{6e^2}e_{\alpha j}F_j\right)\\&+\varepsilon\left(\left(1-\frac{1}{2\tau}\right)\left(\frac{\partial}{\partial \mathrm{t}}+\mathrm{e}_{\alpha j}\frac{\partial}{\partial x_j}\right)f_\alpha^{(1)}=-\frac{1}{\tau}f_\alpha^{(2)}\right.\\&\left.-\frac{1}{2}\left(\frac{\partial}{\partial t}+\mathrm{e}_{\alpha j}\frac{\partial}{\partial x_j}\right)\left(\frac{1}{6e^2}e_{\alpha k}F_k\right)\right)\Bigg].\end{aligned}\tag{27}$$

About α, we have

$$\begin{aligned}&\frac{\partial}{\partial t}\left(\sum_\alpha e_{\alpha i}f_\alpha^{(0)}\right)+\frac{\partial}{\partial x_j}\left(\sum_\alpha e_{\alpha i}e_{\alpha j}f_\alpha^{(0)}\right)+\varepsilon\left(1-\frac{1}{2\tau}\right)\frac{\partial}{\partial x_j}\\&\cdot\left(\sum_\alpha e_{\alpha i}e_{\alpha j}f_\alpha^{(1)}\right)=F_j\delta_{ij}-\varepsilon\frac{1}{2}\sum_\alpha e_{\alpha i}\left(\frac{\partial}{\partial t}+e_{\alpha j}\frac{\partial}{\partial x_j}\right)\\&\cdot\left(\frac{1}{6e^2}e_{\alpha j}F_j\right).\frac{\partial}{\partial \mathrm{t}}\left(\sum_\alpha \mathrm{e}_{\alpha i}\mathrm{f}_\alpha^{(0)}\right)+\frac{\partial}{\partial x_j}\left(\sum_\alpha e_{\alpha i}\mathrm{e}_{\alpha j}f_\alpha^{(0)}\right)\\&+\varepsilon\left(1-\frac{1}{2\tau}\right)\frac{\partial}{\partial x_j}\left(\sum_\alpha e_{\alpha i}e_{\alpha j}f_\alpha^{(1)}\right)=F_j\delta_{ij}\\&-\varepsilon\frac{1}{2}\sum_\alpha e_{\alpha i}\left(\frac{\partial}{\partial t}+e_{\alpha j}\frac{\partial}{\partial x_j}\right)\left(\frac{1}{6e^2}e_{\alpha j}F_j\right).\end{aligned}\tag{28}$$

Again, by using the accuracy of the first order to the force term in Equation ((28)) with reference to LB equation and equilibrium function (Equation ((14))), the remaining terms can be broken down and Equation ((28)) becomes Equation ((2)) which is the momentum equations

$$\begin{aligned}&\underbrace{\frac{\partial}{\partial t}\left(\sum_\alpha e_{\alpha i}f_\alpha^{(0)}\right)}_{\partial(\rho u_i)/\partial t}+\underbrace{\frac{\partial}{\partial x_j}\left(\sum_\alpha e_{\alpha i}e_{\alpha j}f_\alpha^{(0)}\right)}_{\partial\left(\rho u_i u_j\right)/\partial x_j}\\&\underbrace{+\varepsilon\left(1-\frac{1}{2\tau}\right)\frac{\partial}{\partial x_j}\left(\sum_\alpha e_{\alpha i}e_{\alpha j}f_\alpha^{(1)}\right)}_{\Lambda_{ij}}=\underbrace{F_j\delta_{ij}}_{F_i}\\&-\varepsilon\frac{1}{2}\sum_\alpha e_{\alpha i}\left(\frac{\partial}{\partial t}+e_{\alpha j}\frac{\partial}{\partial x_j}\right)\left(\frac{1}{6e^2}e_{\alpha j}F_j\right),\end{aligned}$$

$$\begin{aligned}&\varepsilon\frac{1}{2}\sum_\alpha e_{\alpha i}\left(\frac{\partial}{\partial t}+e_{\alpha j}\frac{\partial}{\partial x_j}\right)\left(\frac{1}{6e^2}e_{\alpha j}F_j\right)=\underbrace{\varepsilon\frac{1}{2}\sum_\alpha\left(\frac{\partial}{\partial t}\frac{1}{6e^2}\overbrace{e_{\alpha i}e_{\alpha j}}^{\sum_\alpha e_{\alpha i}e_{\alpha j}=6e^2\delta_{ij}}F_j\right)}_{0}\\&+\left(e_{\alpha i}e_{\alpha j}\frac{\partial}{\partial x_j}\frac{1}{6e^2}e_{\alpha j}F_j\right)=\underbrace{\varepsilon\frac{1}{12e^2}\frac{\partial}{\partial x_j}\sum_\alpha e_{\alpha i}e_{\alpha j}e_{\alpha j}F_j}_{-(g\partial/\partial x_i)(\rho^2/2)\longrightarrow e_{\alpha j}=e\text{ because }e_{\alpha j}\text{ has the same order as e}}-g\frac{\partial}{\partial x_i}\left(\frac{\rho^2}{2}\right)\longrightarrow e_{\alpha j}=e.\end{aligned}\tag{29}$$

The above equation becomes

$$\frac{\partial(\rho u_i)}{\partial t}+\frac{\partial\left(\rho u_i u_j\right)}{\partial x_j}=g\frac{\partial}{\partial x_i}\left(\frac{\rho^2}{2}\right)-\frac{\partial}{\partial x_j}\Lambda_{ij}+F_i,\tag{30}$$

$$\Lambda_{ij}=\frac{\varepsilon}{2\tau}(2\tau-1)\sum_\alpha e_{\alpha i}e_{\alpha j}f_\alpha^{(1)}.\tag{31}$$

By considering Equation (11) and using LB equation and equilibrium function (Equation (14), results) after some manipulation and algebraic operations, we obtain

$$\Lambda_{ij}\approx-\gamma\left[\frac{\partial(\rho u_i)}{\partial x_j}+\frac{\partial\left(\rho u_j\right)}{\partial x_i}\right].\tag{32}$$

Substituting Equation (32) into Equation (30) gives

$$\frac{\partial(\rho u_i)}{\partial t}+\frac{\partial\left(\rho u_i u_j\right)}{\partial x_j}=-g\frac{\partial}{\partial x_i}\left(\frac{\rho^2}{2}\right)+\gamma\frac{\partial^2(\rho u_i)}{\partial x_j x_j}+F_i,\tag{33}$$

with the kinematic viscosity γ defined as $\gamma=(c^2\Delta t/6)(2\tau-1)$.

2.7. Flow Modeling (LBM). To show from the dynamics of the lattice Boltzmann method that gives a behavior consistent with the Navier-Stokes equations,

$$\begin{aligned}&f_\alpha(X+e_\alpha\varepsilon,t+\varepsilon)-f_\alpha(X,t)=-\frac{1}{\tau}\left(f_\alpha-f_\alpha^{eq}\right)+\frac{\varepsilon}{6e^2}e_{\alpha j}F_j,\\&f_i^{(0)}=\rho t_i\left[1+\frac{u.c_i}{c_s^2}+\frac{uu:c_ic_i}{2c_s^4}-\frac{uu:I}{2c_s^2}\right]\\&\quad=\rho t_i\left[1+\frac{u.c_i}{c_s^2}+\frac{Q_i:uu}{2c_s^4}\right],\\&f_i^{(1)}=-\tau t_i\left(\partial_{t_1}+\nabla_1.c_i\right)\left[\rho+\frac{\rho u.c_i}{c_s^2}+\frac{Q_i:\rho uu}{2c_s^4}\right]\\&\quad=-\tau t_i\left[\partial_{t_1}\rho+\frac{\partial_{t_1}(\rho u.c_i)}{c_s^2}+\frac{\partial_{t_1}(Q_i:\rho uu)}{2c_s^4}\right.\\&\qquad\left.+c_i.\nabla_1\rho+\frac{c_ic_i:\nabla_1(\rho u)}{c_s^2}+\frac{(c_i.\nabla_1)(Q_i:\rho uu)}{2c_s^4}\right],\\&Q_i=c_ic_i-c_s^2I\text{ or }Q_{i\alpha\beta}=c_{i\alpha}c_{i\beta}-c_s^2\delta_{\alpha\beta}.\end{aligned}\tag{34}$$

Recovery of the continuity equation is as follows:

$$\begin{aligned}\frac{\partial\rho}{\partial t}+\nabla\cdot(\rho\cdot V)=0\Rightarrow\partial_{t_1}\rho+\nabla_1\cdot\rho u=0\Rightarrow\partial_{t_1}\sum_i f_i^{(0)}\\+\nabla_1\cdot\sum_i c_i f_i^{(0)}.\end{aligned}\tag{35}$$

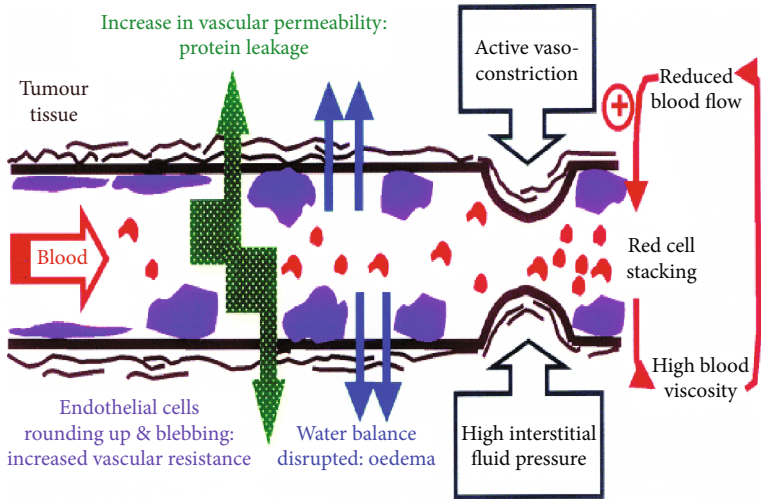

Figure 2: The mechanism of process of angiogenesis in tumor blood vessels.

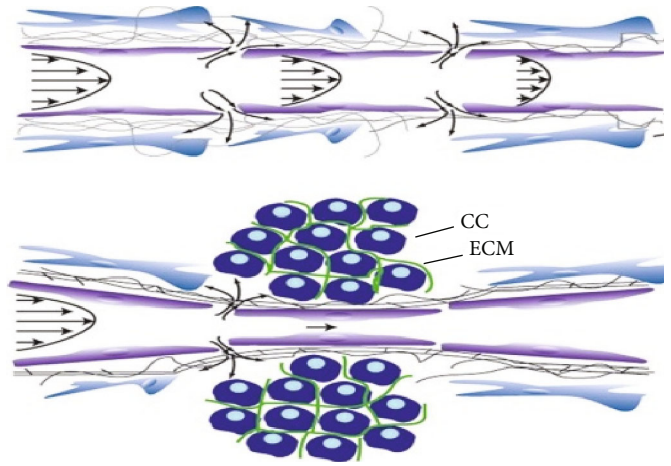

Figure 3: Normal vessel—tumor vessel.

Recovery of the momentum equation is as follows:

$$\nabla\cdot\vec{u}=0\longrightarrow\frac{\partial u}{\partial x}+\frac{\partial v}{\partial y}+\frac{\partial w}{\partial z}=0,$$

$$\rho\left(\frac{\partial\vec{u}}{\partial t}+(u\cdot\nabla)\vec{u}\right)=-\nabla p+\rho\vec{g}+\mu\nabla^2\vec{u},$$

$$\rho(\partial_t u+(u\cdot\nabla)u)+\nabla p-\mu\nabla^2 u-\left(\frac{\mu}{3}+\acute{\mu}\right)\nabla(\nabla\cdot u)=\vec{f},$$

$$\partial_t\rho\vec{u}+\nabla_1\cdot\left[\Pi^{(0)}+\epsilon\Pi^{(1)}+\left(1+\frac{1}{2}\partial_t\right)c_s^2\rho I+\frac{\epsilon}{2}\partial_{t_1}\Pi^{(0)}+\frac{1}{2}\nabla\cdot R^{(0)}\right]=0,$$

$$\Pi^{(0)}=\begin{cases}\Pi^{(0)}=\sum_i Q_i f_i^{(0)}=\sum_i\left(c_i c_i-c_s^2 I\right)f_i^{(0)},\\ \Pi^{(0)}_{\alpha\beta}=\dfrac{\rho^2}{2}\left[u_\gamma u_\delta\left(\delta_{\alpha\gamma}\delta_{\beta\delta}+\delta_{\alpha\delta}\delta_{\beta\gamma}\right)\right]=\dfrac{\rho}{2}\left(u_\alpha u_\beta+u_\alpha u_\beta\right)=\rho u_\alpha u_\beta,\\ \Pi^{(0)}=\rho uu,\end{cases}$$

$$\nabla\cdot R^{(0)}=\begin{cases}\nabla\cdot R^{(0)}=\nabla\cdot\sum_i c_i c_i c_i f_i^{(0)},\\ \left\{\nabla\cdot R^{(0)}\right\}_{\alpha\beta}=\partial_\gamma\sum_i c_{i\alpha}c_{i\beta}c_{i\gamma}f_i^{(0)},\\ \nabla\cdot R^{(0)}=c_s^2\left[(\nabla\cdot\rho u)I+\nabla\rho u+(\nabla\cdot\rho u)^T\right],\end{cases}$$

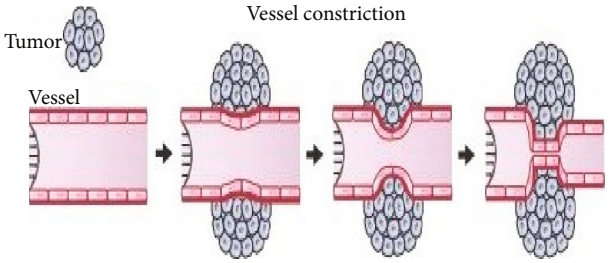

Figure 4: Tumor-vessel interaction.

$$\Pi^{(1)}=\sum_i Q_i f_i^{(1)}=\sum_i\left(c_i c_i-c_s^2 I\right)f_i^{(1)},$$

$$f_i^{(1)}=f_i^{(1)}=\frac{-\tau t_i}{c_s^2}\cdot\left[Q_i:\rho(\nabla_1 u)-c_i\nabla_1:(\rho uu)+\frac{1}{2c_s^2}(c_i\cdot\nabla_1)(Q_i:\rho uu)\right],$$

$$\Pi^{(1)}=-\tau\rho c_s^2\left[\nabla_1 u+(\nabla_1 u)^T\right],$$

$$\partial_{t_1}\Pi^{(0)}=-c_s^2[(\nabla_1\rho)u+u(\nabla_1\rho)],$$

$$\{\nabla\cdot\rho I\}_\alpha=\partial_\beta p\delta_{\alpha\beta}=\partial_\beta p=\{\nabla\cdot p\}_\alpha\longrightarrow\nabla\cdot pI=\nabla p.\tag{36}$$

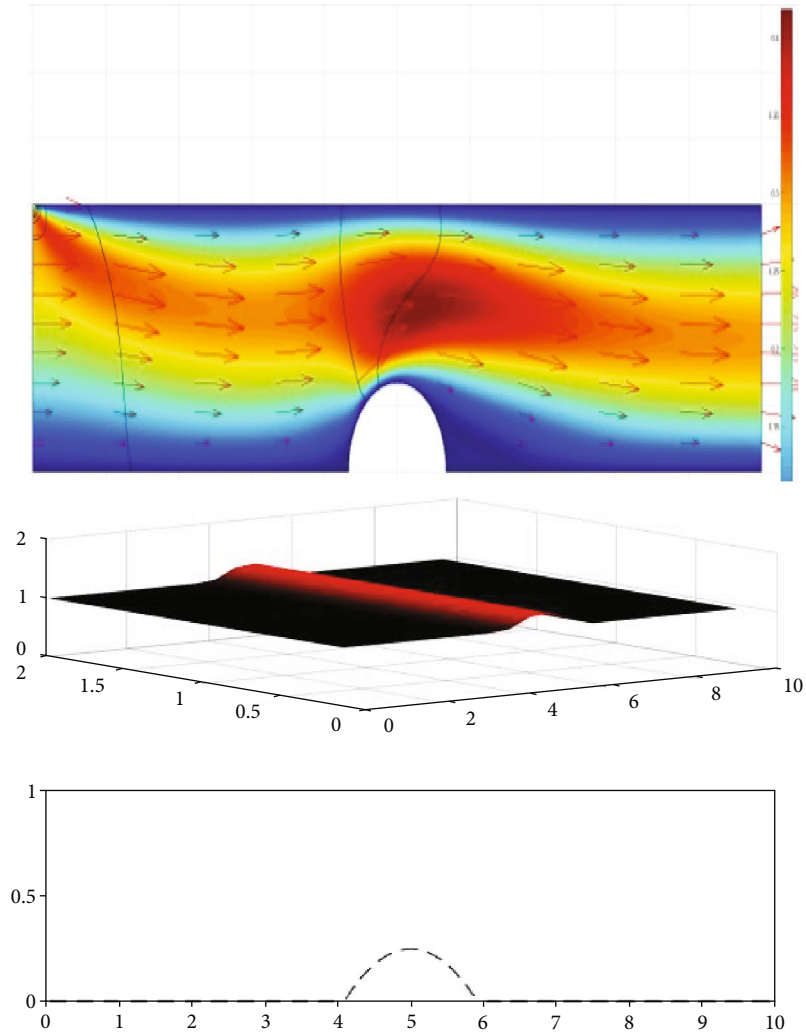

Figure 5: An arterial stenosis' flow geometry with 1/3*D*.

Inserting all the unknown terms into

$$\partial_t \rho \vec{u} + \nabla_1 \cdot \left[\Pi^{(0)} + \epsilon \Pi^{(1)} + \left(1 + \frac{1}{2}\partial_t\right) c_s^2 \rho I + \frac{\epsilon}{2} \partial_{t_1} \Pi^{(0)} + \frac{1}{2} \nabla \cdot R^{(0)} \right] = 0 \tag{37}$$

gives

$$\partial_t \rho u + \nabla \cdot \left[\rho uu - \tau \rho c_s^2 \left(\nabla u + (\nabla u)^T + \rho I + \frac{c_s^2}{2} \partial_t \rho I \right. \right.$$
$$\left. \left. - \frac{c_s^2}{2} \left([\nabla \rho] u + u[\nabla \rho] + \frac{c_s^2}{2} \left(\nabla \cdot [\rho u] I + \nabla \nabla \rho u + [\nabla u]^T \right) \right] = 0. \right. \tag{38}$$

3. Numerical Results and Discussion

3.1. Discussion. Modeling of tumor blood vessels (modeling of solid tumor invasion (growth)) is typically a challenging task. This work focuses on the mathematical framework and computational solution methodology through numerical simulation for the blood flow (perfusion) patterns inside vascular networks with the solid tumors (in tumor vessels) plug away at the effects of vessel leakiness and compression. During the process of angiogenesis, cancer tumors are supplied with fresh oxygen and nutrients as well as blood flow in the networks of vasculature to find the routes of metastasizing cancer cells. With regard to cancer, a process of angiogenesis allows tumors to grow in an irregular form, its function being characterized by abnormal endothelial cell stratification and altered basement membranes, creating large gaps between endothelial cells of the vasculature and blood vessel tortuosity, and metastasize or host tissue invasion phase. While the process of angiogenesis is induced in tumors, it commonly leads to poorly set up of vasculature with several issues, namely, particularly leakiness (the leakage of blood plasma carries off to an increase in the interstitial pressure. This leads to the artery burst, whereas in a narrow artery, there is a risk of the blood being blocked in greater amount leading to erratic blood flow which has the consequence of poor blood circulation in the downstream. Thus, it results in the vessel occlusion and acute hypoxia and excessive and convoluted branching of blood vessels that leads to the persisting release of VEGF. Abnormalities in various components of the tumor

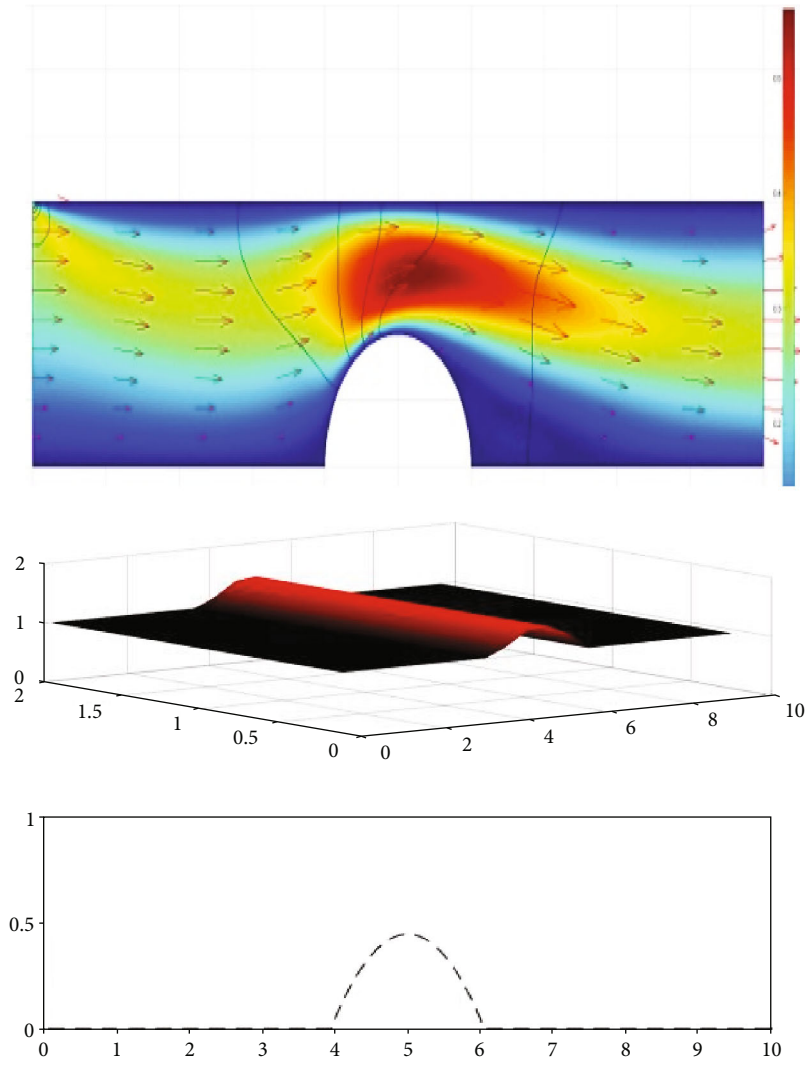

Figure 6: An arterial stenosis' flow geometry with 1/2*D*.

vessel wall have been caused by various changes in the structure of the vessel's diameter in the hierarchy of arterioles, capillaries, and venules. This provided the hyperpermeability of the tumor vessels and generates a couple of topological changes such as the forming hypovascular and hypervascular regions inside the tumors as well as in the adjoining areas [73].

In the presence of the avascular growth phase, the vasculature begins to grow rapidly as well as often chaotically, and its poor function leads to tumor vasculature lacking in the conventional hierarchy of blood vessels. Thus, the large subsets of tumor cells become deprived of nutrients and oxygen. The deformability of the vessel geometry, tumor vasculature, and artery wall such as rupture (stenosed) with any blood composition under stresses denotes the wall shear stresses inside the tumor. These demonstrate the lowdown of oxygen to a tumor that could possibly become a more aggressive tumor which is vulnerable for more high risk and damage the oxygenated one [74, 75]. The blood flow through the network of solid tumors leads to arterial stenosis and the hydrostatic stress (generated by the growing tumor). Thus, the stenosis in the artery is generated by the growth and movement of solid tumors and mediated by hydrostatic stress, and as the consequence, the hydrostatic stress affects vascular remodeling by restricting the radii of the vessels. Thus, mathematically, arterial stenosis is vascular compression, and this phenomenon reduces the effective cross-sectional area of tumor blood vessels by the constriction and collapse of vessels which can result in insufficient blood supply to the tissues downstream region of stenosis.

The vessel geometry and the dynamic behavior of blood flow in the vascular network affected by tumor growth play decisive roles in the formation of atherosclerosis, arterial stenosis, and hypoxia (deficiency in the amount of oxygen reaching the tissues), as seen in Figure 1. The computational fluid dynamics (CFD) techniques, mathematical modeling, and biophysically justified computer models are valuable tools with great potential in biofluid research, due to the fact that they are widely applied under complex fluid dynamics issues related to medical research. The ultimate aim of those scientific research is to aid to figure out the mechanisms of the diagnosis and treatment of these diseases or even control the progression of the disease [76].

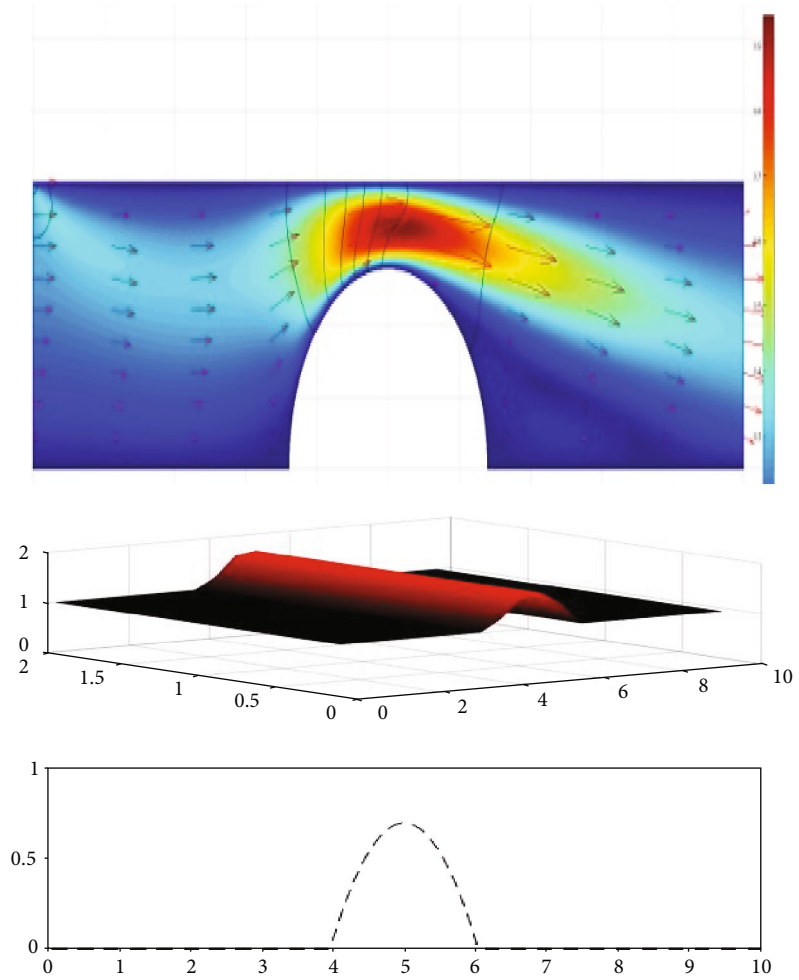

Figure 7: An arterial stenosis' flow geometry with 2/3*D*.

In accordance with the size and the dimensional irregularities of vessel diameters, one can see a drastic change in the blood viscosity in the aftermath of arterial stenosis or solid pressure that further decreases blood vessel diameter and presents high viscosity of blood, enhancing the friction between RBCs and endothelial cells, intensifying at high hematocrit (see Figure 2). The viscosity of blood that flows through the arteries does not behave as a continuum, slow and steady. The blood flow is a kind of non-Newtonian fluid flow such that viscosity of blood can change systematically when it is subjected to force; it deforms either as more liquid or more solid. The viscosity for the non-Newtonian flow displays the shear-thinning feature close to the wall. The viscoelastic properties which make human blood non-Newtonian depend on blood cell distribution, the elastic behavior of red blood cells, and the aggregation of red cells cause the blood clotting to happen [77].

In consequence, the ambient physical conditions like shearing, extensional, and any deformation forces have an impact on the blood viscosity. The viscosity of blood has an inverse correlation with the Reynolds number (Re) whenever fluid behaves as a Newtonian, which can be seen when the viscosity nonlinearly decreases when Re increases. Based on the experimental studies on non-Newtonian fluid, it could be tough to determine the viscosity for the Reynolds number [12]. The Reynolds number is used to categorize the fluid systems in which the effect of viscosity is crucial in controlling the velocities, the flow pattern of a fluid, clotting, and arterial thrombosis [78, 79].

3.2. Validation of Model. The data of Sun and Munn [48], Liu [71], and Harrison [72] are used to verify the current LBM results with the help of the lattice nodes in the computational domain, flow parameters, and initial and boundary conditions (bounce-back boundary condition is imposed at the walls; corresponding to a nonslip wall boundary condition, the flow velocities at the inlets are imposed). To compare the numerical results (obtained from LBM) with the numerical data of Tan [80], two results were randomly picked to obtain the maximum absolute error (MAXE) as 9.8492×10^{-4} and the global relative error (GRE) as 1.4295×10^{-4}. In most cases, the initial validation not only showed good code performance, but also it exhibits good agreement with the referred data. It can be concluded that the LB method performs with the present research problem. The numerical results agree with the theory; hence,

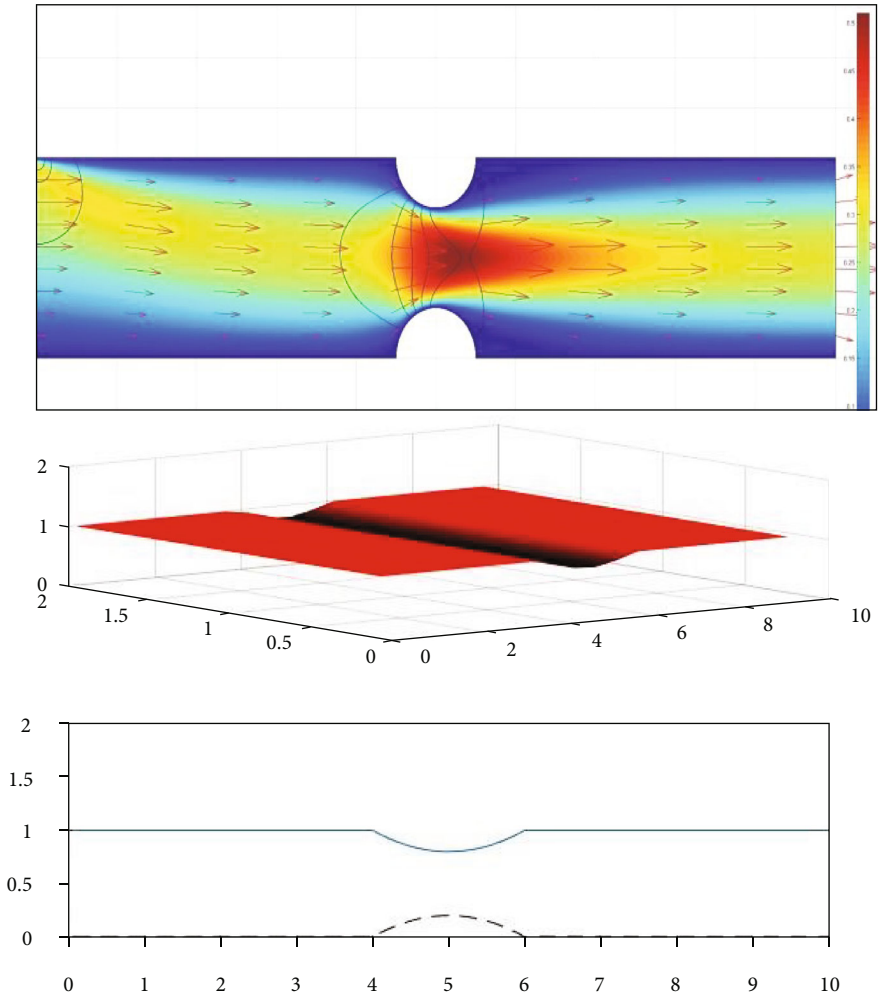

Figure 8: An arterial stenosis' flow geometry with 1/4*D*.

the stability analysis is a good tool for designing the LB method.

3.3. Numerical Scheme. In the solution methodology of this study, the lattice Boltzmann method has been applied to simulate the nonlinear incompressible blood flow in a complex microvascular network. It has been noted that a wide range of problems of nonlinear incompressible fluid flow are within the dynamics range of the LBM and the utilization of this technique has been affirmed. The use of LBM provides the flexibility to study the effects of blood flow in complex microvascular networks by explicitly accounting for RBC aggregation, leukocyte-endothelium interactions, and cell-cell interactions [81, 82].

To demonstrate the potential of the NS-LBM approach and its appropriateness for the application, three benchmark problems that are widely come across in the model of solid tumor growth are investigated. Regarding the models, the work presented here plans to progress with better accuracy and develop additional information analysis of the impact of blood flow and interstitial flow through solid pressure and stenotic vessels which along with the constriction and collapse of vessels across capillary walls or in microvascular networks (the solid pressure on blood vessel dynamics) as shown in Figures 3 and 4.

In order to investigate on how the variability in the size of vessel diameter is connected to changes in the high leakiness of vessels in the lack of lymphatic function which leads to create an elevated interstitial pressure and compression (the solid pressure generated by the growing tumor and flows in tumor-induced vascular networks) of tumor blood vessels, three test cases of generic stenosis geometries are constructed and designed.

3.4. Cases of a Stenosis through the Vessel Diameter. The computational domain (as depicted in Figures 5–13) is composed of a 3D blood vessel with stenosis across the capillary walls, and flow happens between upper and lower walls. The stenosis is axially symmetric with diverse occlusion percentages of 1/3*D*, 1/2*D*, 2/3*D* or 1/4*D*, 1/3*D*, 1/2*D* located 2D far from each other's, where *D* is the blood vessel's diameter. The unidirectional steady flow of blood in the stenotic artery is considered and is along the longitudinal direction (along *x*-axis).

In order to use the test cases for the lattice Boltzmann method, an accurate description of the model's parameter

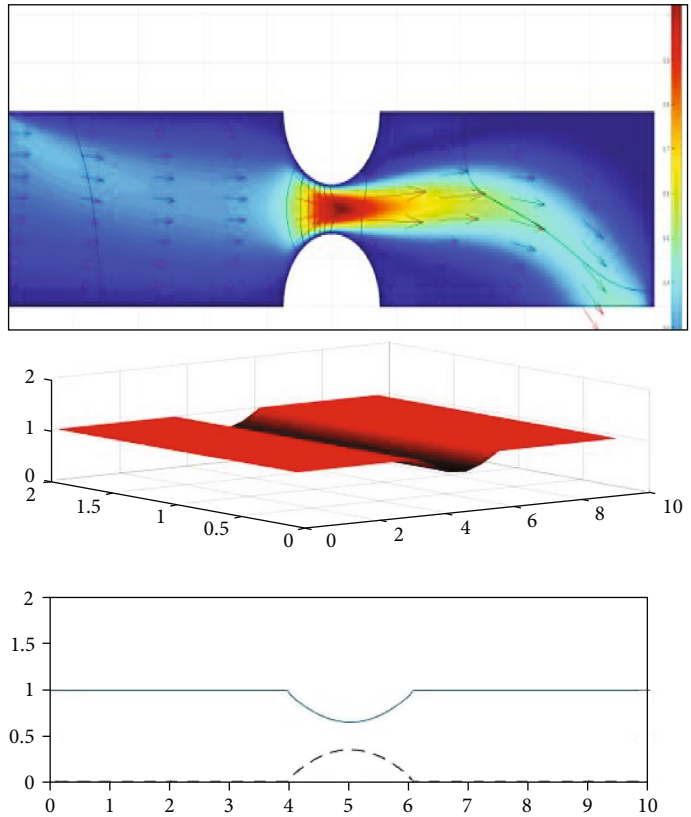

Figure 9: An arterial stenosis' flow geometry with 1/3*D*.

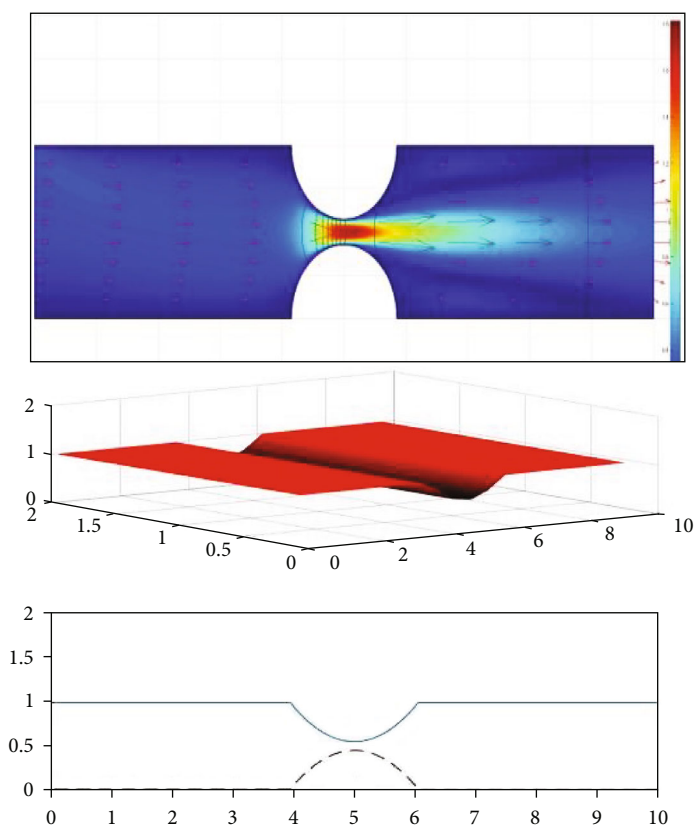

Figure 10: An arterial stenosis' flow geometry with 2/3*D*.

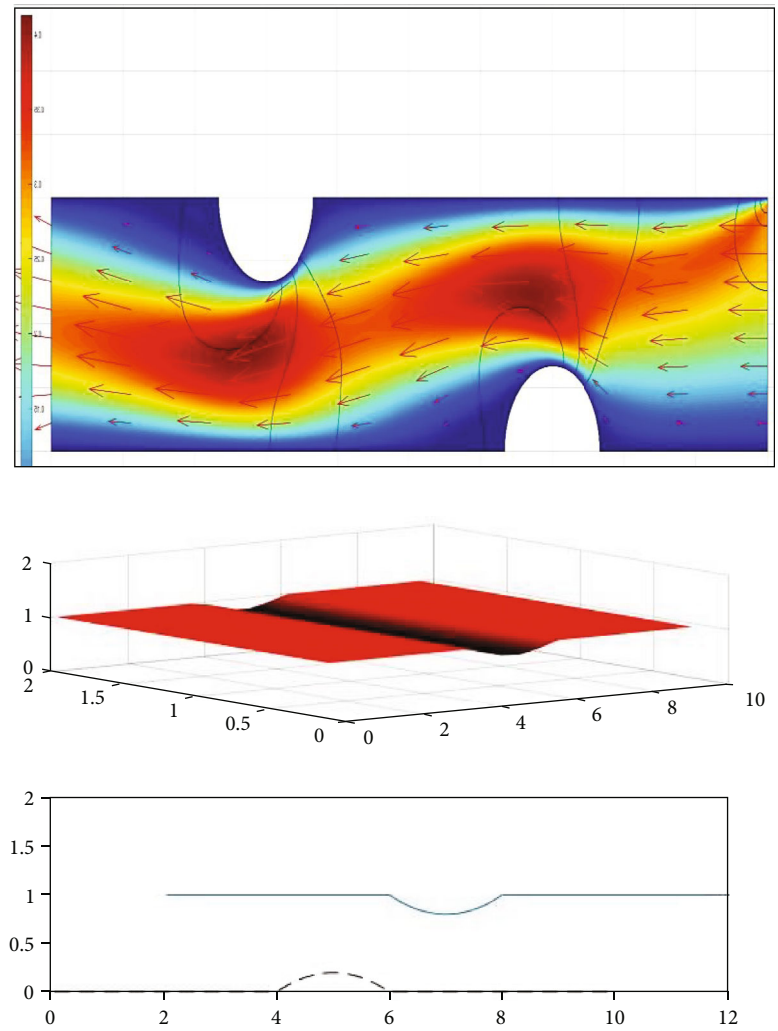

Figure 11: An arterial stenosis' flow geometry with 1/3*D*.

such as the parameters' range and units, lattice sizes, and relaxation time is required. The D2Q9 velocity model is used to study the problem of blood flow in stenosed artery. The results further indicate that when lattice sizes become smaller, better results are obtained. Since the results based on $\Delta x \leq 0.05$ m provides better and more accurate solutions, the model is conservative and accurate. The method implored is sensitive to the choice of values for the single relaxation time over the range considered. For single relaxation time $\tau < 1$, LBM will not be stable and generate unphysical oscillations. For a single relaxation time $\tau \gg 1$, LBM will be stable and depend on value which shows different quantity. To achieve a lattice-independent solution, a lattice of grid size 15,000 × 6,000 with speed $e = 200$ m/s is used. In this simulation, the vessel diameter has 40 lattice nodes and the length has 80 lattice nodes. The LBM is a discrete numerical method; it may suffer instability like any other numerical method, but by using suitable time relaxation values, lattice size, and time step (iterations), such instabilities could be minimized. Also, another option that is important for the stability of LBM is kinematic viscosity. The kinematic viscosity υ must be positive $\upsilon = (2\tau - 1)/6 > 0$. In these three test problems, we assume the density ρ as constant and choose it as $\rho = 1$. The steady-state solution tends to be accurate after the 2,000th iteration. It has been apparent that when the Re number increases, the non-Newtonian fluid viscosity nonlinearly decreases. For the non-Newtonian fluids, blood flow behaves as a non-Newtonian fluid flow through stenosed blood vessels with viscosity μ in the range 0.001-1.0.

Moreover, for modeling tumor blood vessels with LBM, appropriate boundary conditions must be selected since the solutions should be compatible with the physical constraints and the inherent nature/regime of the flow. The slip boundary condition is applied at the side walls. Results are plotted using the inflow and outflow scheme as seen in the figures and codes. The slip or nonslip boundary conditions are handled at the solid walls (solid walls: nonslip velocity). For the nonslip condition, the bounce-back scheme is imposed, and for slip conditions, a zero gradient of the distribution function normal to the solid wall is applied. Periodic boundary conditions were used in the upper and lower walls. Furthermore, a bounce-

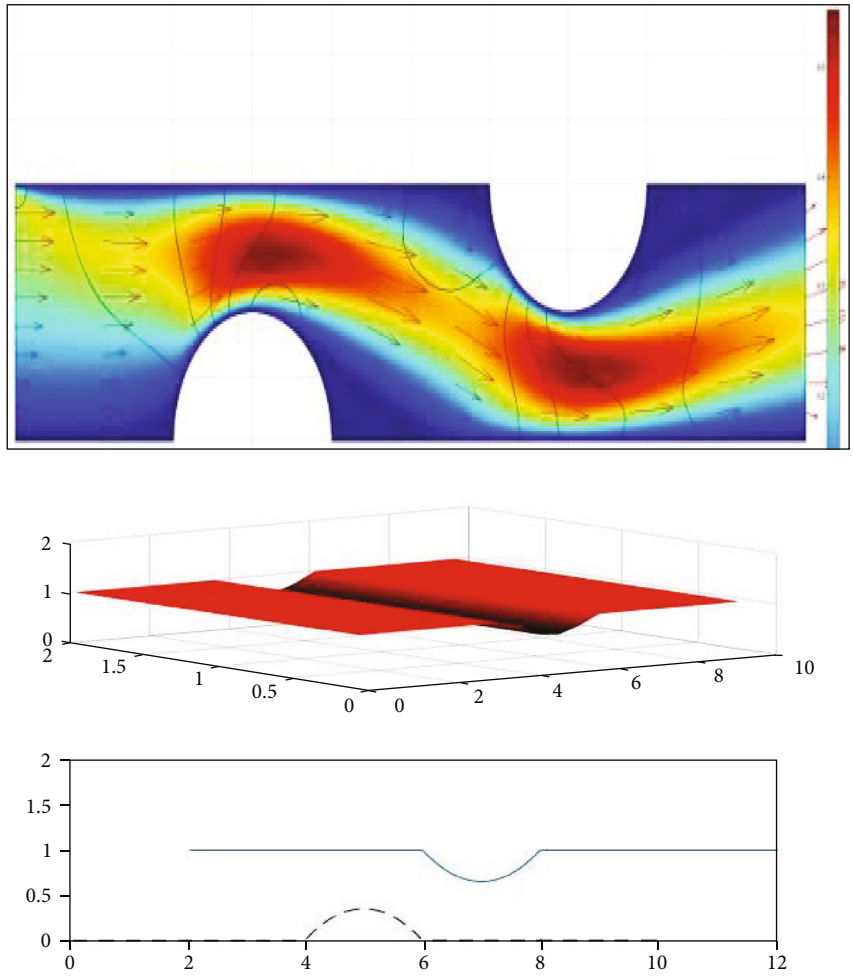

Figure 12: An arterial stenosis' flow geometry with 1/2D.

back boundary condition acts as a nonslip wall boundary condition applied at walls.

The streamlines of blood flow through a microchannel (vessel) with stenosis and other snapshots of the schematic of the model in Cartesian coordinate system are simulated using the LBM. The result shows the geometry, motion of the flow of blood in small vessels, inlet and outlet velocity, and deformation of arterial stenosis.

The results of several different flow velocities are presented in Figures 5–13. It becomes apparent with the minor variation of depth in the stenosed vessel; the blood flow velocity convergence can be transitional or turbulent that depends on the diameter of stenosis of the artery, directions, and geometry. Whenever the depth of stenosis of the artery is 1/3 D of depth in the vessel, a higher flow velocity can be observed at the center of the stenosis (at the crest), which is 0.4 ms^{-1}. The mainstream flows parallel to the center of this vessel and instantaneously at the downstream of the stenosis; the outflow velocity field becomes steady. By increasing the depth of the stenosis to 1/2D of depth in the vessel, the maximum velocity is over 0.6 ms^{-1}, slightly higher than the maximum velocity of the previous case. A higher flow velocity and intensified results can be found when the depth of the stenosis increased to 2/3 D of depth in the vessel, where it approached $\sim 1\ \text{ms}^{-1}$. The downstream tissues have insufficient blood supply; moreover, risk factors for these kinds of stenosis include high blood pressure and high cholesterol when the solid pressure is high. Figures 5–7 show the number of snapshots of the free surface elevation during the propagation of the blood flow velocity test case.

Figures 8–10 show the generic stenosis geometries with different occlusion percentages in the opposite directions of both the top and bottom walls. By increasing the diameter of the stenosis from 1/4D, 1/3D, and 2/3 D, the results show that the blood flow velocities' raise will be significant in the area between the occlusions, where they approach from 0.5 ms^{-1} to $\sim 1.8\ \text{ms}^{-1}$ that a higher flow velocity will cause faster advection. As a consequence of radical change (revolutionary change), the blood flow of red cell reduces remarkably and leads to blood clotting too fast with high blood viscosity. Peak turbulence intensities are present for the present cases, the blood flow velocity is intensively concentrated in the center of the vessel, and the highest wall shear stress exists in the geometry.

According to the results, there exist two regions of highly concentrated stresses, and these areas may possess the

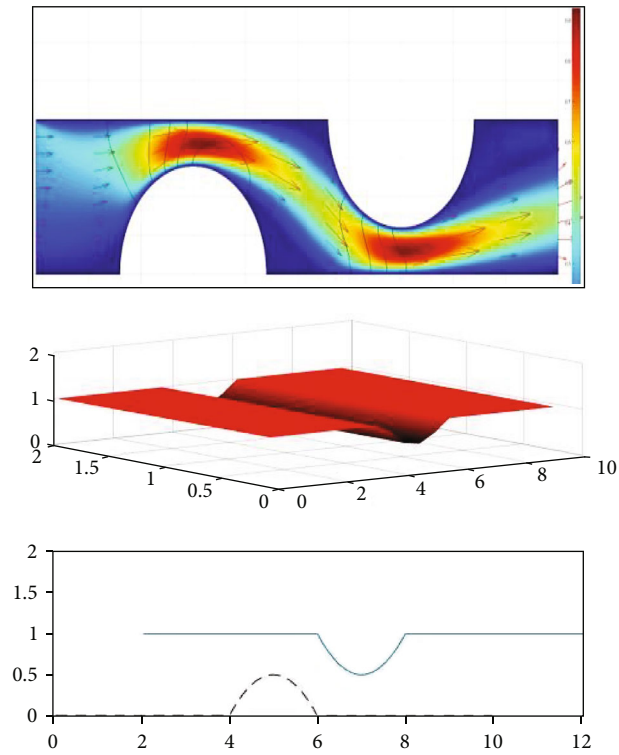

Figure 13: An arterial stenosis' flow geometry with 2/3D.

highest risk of rupture. In consonance with the high-stress regions, it may pose severe problems if they exceed the allowable stress level causing the wall to deform. With regard to the dynamics of the blood, the vortex intensity is relatively high behind the narrow area.

Figures 11–13 depict the three cases of tests with different generic stenosis geometry occlusions with the stenosis diameter from 1/3D, 1/2D, and 2/3 D with two-sided constricted vessel and 2D distances from each other. The peak velocity is highly increased in two regions on the top of the stenosis and vortices near the top of the stenotic parts as well. By increasing the diameter of the stenosis and minimizing the distances between the stenosis, two distinct recirculation regions appear near the postlip of the stenosis due to the separation of the shear layer induced by the stenosis. In the region of the stenosis, the amount of blood flow decreases, and the turbulent intensity of the flow increases significantly, so the flow recirculates and an adverse streamwise pressure gradient exists near the walls.

According to the information provided by the researchers and the research carried out on blood flow, the viscosity for the non-Newtonian fluid flow displays the shear-thinning feature close to the wall that it depends on the geometry and the Reynolds number, and high viscosity is observed in some cases, in terms of preventing any deviations and oscillation on plots and demonstrating the velocity being stable. The Reynolds number tested was set between 20 and 1,500 that is dependent on the test cases. The typical Reynolds number for the blood flow varies; in small arteries, it starts to range from 1000 to 4,000 in large diameter arteries; meanwhile, based on the experimental studies on non-Newtonian fluid, it could be tough to determine the proper viscosity for the Re number [12] in small diameter arteries. Blood flow always shows unsteady (pulsatile) nature, and blood pressure fluctuates continuously due to the cyclic nature of the pumping action of the heart. When blood flows through small diameter arteries (<300 μm), it exhibits non-Newtonian fluid's character. The Reynolds number range 20-1,000 is estimated; when blood flows in stenosed narrow blood vessels, the rate of Re reduced up to 50% at the area of reduction. In the downstream region of the stenosis, when the flow becomes transition-to-turbulent, it is evident that the Re numbers are in the high-frequency range and have revealed a high level of turbulence.

4. Conclusions

This research paper analyzed the blood vessel dynamics modeling in the presence of tumor and/or stenosis, by applying, verifying, and affirming LBM as an invaluable numerical modeling and simulation method. The model result shows that the flow features are extremely sensitive to stenosis severity, even at small strains and stresses, and that a severe effect on flow patterns and wall shear stresses is noticed in the tumor blood vessels. The results obtained in this study reveal a useful information on describing blood vessel deformations more precisely. The results obtained are beneficial to realize the impacts of the geometrical complexity factors on the natural blood flow rates through the bucked shapes. It also exhibits the various biological properties, blood vessel deformability, and severe cardiovascular diseases.

It is found that based on the nonlinear deformation of the blood vessel's wall, the flow rate conditions became unstable or distorted and affect the complex blood vessel's geometry and it changes the blood flow pattern. When the blood flows inside the stenotic artery, depending on the presence of moderate or severe stenosis, it can lead to insufficient blood supply to the tissues in the downstream. Consequently, the highly disturbed flow occurs in the downstream of the stenosed artery, or even plaque ruptures happen when the flow pattern becomes very irregular and complex as it transits to turbulent which cannot be described without assumptions on the geometry.

The lattice Boltzmann (LB) method is a sophisticated and powerful computational tool which can simulate the blood flow through stenosed arteries under steady and pulsatile states, treating it as non-Newtonian fluid. Thus, the LB method presents the results professionally and estimates the numerical solution with high accuracy even to nonlinear flow problems. The outcomes of test cases (given in Section 3.3) provide vital information about stenosis in the vessel with solid tumor. Thus, this computational model provides significant results which could be beneficial to the clinician as well as to the patient, and in fact, these results may guide the society for efficiently searching the efficient and optimal individualized treatment strategies that can include chemotherapeutic procedures and adjuvant treatments like antiangiogenic (drugs).

Nomenclature

g: Gravity acceleration vector
t: Time
p: Blood pressure
i: Cartesian indices
j: Einstein's summation
u_i: ith direction-average depth velocity
∇: Vector differential operator
$\boldsymbol{u} = (u, v, w)$: $u\boldsymbol{i} + v\boldsymbol{j} + w\boldsymbol{k}$
ν: Kinematic viscosity
μ: Dynamic viscosity (blood)
ρ: Density (blood) ~ ρ_{blood} 1060 kgm^3).

Data Availability

The numerical data are included within the article.

Conflicts of Interest

The authors report that there are no competing interests to declare.

References

[1] J. N. Blattman and P. D. Greenberg, "Cancer immunotherapy: a treatment for the masses," *Science*, vol. 305, no. 5681, pp. 200–205, 2004.

[2] C. R. Parish, "Cancer immunotherapy: the past, the present and the future," *Immunology and Cell Biology*, vol. 81, no. 2, pp. 106–113, 2003.

[3] A. Moretta, "Natural killer cells and dendritic cells: rendezvous in abused tissues," *Nature Reviews Immunology*, vol. 2, no. 12, pp. 957–964, 2002.

[4] T. Alarcón, H. M. Byrne, and P. K. Maini, "A multiple scale model for tumor growth," *Multiscale Modeling & Simulation*, vol. 3, no. 2, pp. 440–475, 2005.

[5] D. Lee, H. Rieger, and K. Bartha, "Flow correlated percolation during vascular remodeling in growing tumors," *Physical Review Letters*, vol. 96, no. 5, 2006.

[6] K. Bartha and H. Rieger, "Vascular network remodeling via vessel cooption, regression and growth in tumors," *Journal of Theoretical Biology*, vol. 241, no. 4, pp. 903–918, 2007.

[7] M. Welter, K. Bartha, and H. Rieger, "Emergent vascular network inhomogeneities and resulting blood flow patterns in a growing tumor," *Journal of Theoretical Biology*, vol. 250, no. 2, pp. 257–280, 2008.

[8] D. Balding and D. L. S. McElwain, "A mathematical model of tumour-induced capillary growth," *Journal of Theoretical Biology*, vol. 114, no. 1, pp. 53–73, 1985.

[9] N. V. Mantzaris, S. Webb, and H. G. Othmer, "Mathematical modeling of tumor-induced angiogenesis," *Journal of Mathematical Biology*, vol. 49, no. 2, pp. 111–187, 2004.

[10] M. A. J. Chaplain, S. R. McDougall, and A. R. A. Anderson, "Mathematical modeling of tumor-induced angiogenesis," *Annual Review of Biomedical Engineering*, vol. 8, no. 1, pp. 233–257, 2006.

[11] M. E. Orme and M. A. J. Chaplain, "A mathematical model of vascular tumour growth and invasion," *Mathematical and Computer Modelling*, vol. 23, no. 10, pp. 43–60, 1996.

[12] X. Zheng, S. M. Wis, and V. Cristini, "Nonlinear simulation of tumor necrosis, neo-vascularization and tissue invasion via an adaptive finite-element/level-set method," *Bulletin of Mathematical Biology*, vol. 67, no. 2, pp. 211–259, 2005.

[13] A. R. A. Anderson and M. A. J. Chaplain, "Continuous and discrete mathematical models of tumor-induced angiogenesis," *Bulletin of Mathematical Biology*, vol. 60, no. 5, pp. 857–899, 1998.

[14] A. R. A. Anderson, K. A. Rejniak, P. Gerlee, and V. Quaranta, "Modelling of cancer growth, evolution and invasion: bridging scales and models," *Mathematical Modelling of Natural Phenomena*, vol. 2, no. 3, pp. 1–29, 2008.

[15] P. Gerlee and A. R. A. Anderson, "An evolutionary hybrid cellular automaton model of solid tumour growth," *Journal of Theoretical Biology*, vol. 246, no. 4, pp. 583–603, 2007.

[16] P. Gerlee and A. R. A. Anderson, "A hybrid cellular automaton model of clonal evolution in cancer: the emergence of the glycolytic phenotype," *Journal of Theoretical Biology*, vol. 250, no. 4, pp. 705–722, 2008.

[17] P. Gerlee and A. R. A. Anderson, "Evolution of cell motility in an individual-based model of tumour growth," *Journal of Theoretical Biology*, vol. 259, no. 1, pp. 67–83, 2009.

[18] V. Cristi, H. B. Frieboe, R. Gatenby, S. Casert, M. Ferrar, and J. Sine, "Morphologic instability and cancer invasion," *Clinical Cancer Research*, vol. 11, no. 19, pp. 6772–6779, 2005.

[19] J. E. Schmitz, A. R. Kansal, and S. Torquato, "A cellular automaton model of brain tumor treatment and resistance," *Journal of Theoretical Medicine*, vol. 4, no. 4, pp. 223–239, 2002.

[20] W. Duchting and G. Dehl, "Spatial structure of tumor growth: a simulation study," *IEEE Transactions on Systems, Man, and Cybernetics*, vol. 10, no. 6, pp. 292–296, 1980.

[21] W. Duchting and T. Vogelsaenger, "Three-dimensional pattern generation applied to spheroidal tumor growth in a nutrient medium," *International Journal of Bio-Medical Computing*, vol. 12, no. 5, pp. 377–392, 1981.

[22] W. Duchting and T. Vogelsaenger, "Aspects of modelling and simulating tumor growth and treatment," *Journal of Cancer Research and Clinical Oncology*, vol. 105, no. 1, pp. 1–12, 1983.

[23] W. Duchting, T. Ginsberg, and W. Ulmer, "Modelling of tumor growth and treatment," *Zeitschrift Fur Angewandte Mathematik Und Mechanik*, vol. 76, pp. 347–350, 1996.

[24] A. R. Kansal, S. Torquato, G. R. Harsh, E. A. Chiocca, and T. S. Deisboeck, "Simulated brain tumor growth dynamics using a three-dimensional cellular automaton," *Journal of Theoretical Biology*, vol. 203, no. 4, pp. 367–382, 2000.

[25] J. Metzcar, Y. Wang, R. Heiland, and P. Macklin, "A review of cell-based computational modeling in cancer biology," *JCO Clinical Cancer Informatics*, vol. 2, no. 3, pp. 1–13, 2019.

[26] P. Macklin and M. E. Edgerton, *Discrete Cell Modeling, 88–122*, Cambridge University Press, Cambridge, UK, 2010.

[27] H. Hatzikirou and A. Deutsch, "Cellular automata as microscopic models of cell migration in heterogeneous environments," *Current Topics in Developmental Biology*, vol. 81, pp. 401–434, 2008.

[28] Y. Jiang, J. Pjesivac-Grbovic, C. Cantrell, and J. P. Freyer, "A multiscale model for a vascular tumor growth," *Biophysical Journal*, vol. 89, no. 6, pp. 3884–3894, 2005.

[29] H. B. Frieboes, J. S. Lowengrub, S. Wise, X. Zheng, P. Macklin, and V. Cristini, "Computer simulation of glioma growth and morphology," *NeuroImage*, vol. 37, no. S1, pp. S59–S70, 2007.

[30] J. Lowengrub, H. Frieboes, F. Jin et al., "Nonlinear modelling of cancer: bridging the gap between cells and tumours," *Nonlinearity*, vol. 23, no. 1, pp. R1–R91, 2010.

[31] T. S. Deisboeck and G. S. Stamatakos, *Multiscale Cancer Modeling*, CRC Press, Boca Raton, FL, USA, 2010.

[32] E. Gavagnin and C. A. Yates, *Stochastic and Deterministic Modeling of Cell Migration*, Elsevier, Amsterdam, Netherlands, 2018.

[33] H. M. Byrne, "Dissecting cancer through mathematics: from the cell to the animal model," *Nature Reviews Cancer*, vol. 10, no. 3, pp. 221–230, 2010.

[34] H. Xie, Y. Jiao, Q. Fan et al., "Modeling three-dimensional invasive solid tumor growth in heterogeneous microenvironment under chemotherapy," *PLoS One*, vol. 13, no. 10, article e0206292, 2018.

[35] Y. Jiao and S. Torquato, "Emergent behaviors from a cellular automaton model for invasive tumor growth in heterogeneous microenvironments," *PLoS Computational Biology*, vol. 7, no. 12, article e1002314, 2011.

[36] Y. Jiao and S. Torquato, "Evolution and morphology of microenvironment- enhanced malignancy of three-dimensional invasive solid tumors," *Physical Review E*, vol. 87, no. 5, article 052707, 2013.

[37] J. Smolle and H. Stettner, "Computer simulation of tumour cell invasion by a stochastic growth model," *Journal of Theoretical Biology*, vol. 160, no. 1, pp. 63–72, 1993.

[38] J. Smolle, H. W. Rainer, K. Regina, C. Lorenzo, H. Josef, and K. Helmut, "Computer simulations of histologic patterns in melanoma using a cellular automaton provide correlations with prognosis," *Journal of Investigative Dermatology*, vol. 105, no. 6, pp. 797–801, 1995.

[39] S. C. Ferreira, M. L. Martins, and M. J. Vilela, "A growth model for primary cancer," *Physica A: Statistical Mechanics and its Applications*, vol. 261, no. 3-4, pp. 569–580, 1998.

[40] H. Hatzikirou, L. Brusch, C. Schaller, M. Simon, and A. Deutsch, "Prediction of traveling front behavior in a lattice-gas cellular automaton model for tumor invasion," *Computers & Mathematics with Applications*, vol. 59, no. 7, pp. 2326–2339, 2010.

[41] O. Pelliccioni, M. Cerrolaza, and M. Herrera, "Lattice Boltzmann dynamic simulation of a mechanical heart valve device," *Mathematics and Computers in Simulation*, vol. 75, no. 1-2, pp. 1–14, 2007.

[42] M. Krafczyk, M. Cerrolaza, M. Schulz, and E. Rank, "Analysis of 3D transient blood flow passing through an artificial aortic valve by lattice-Boltzmann methods," *Journal of Biomechanics*, vol. 31, no. 5, pp. 453–462, 1998.

[43] X. J. Zhang, X. Y. Li, and F. He, "Numerical simulation of blood flow in stented aneurysm using lattice Boltzmann method," in *7th Asian-Pacific Conference on Medical and Biological Engineering. IFMBE Proceedings*, vol. 19, pp. 113–116, Berlin, Heidelberg, 2008.

[44] R. Ouared, B. Chopard, B. Stahl, D. A. Rüfenacht, H. Yilmaz, and G. Courbebaisse, "Thrombosis modeling in intracranial aneurysms: a lattice Boltzmann numerical algorithm," *Computer Physics Communications*, vol. 179, no. 1-3, pp. 128–131, 2008.

[45] M. Hirabayashi, M. Ohta, D. A. Rüfenacht, and B. Chopard, "A lattice Boltzmann study of blood flow in stented aneurism," *Future Generation Computer Systems*, vol. 20, no. 6, pp. 925–934, 2004.

[46] R. Ouared and B. Chopard, "Lattice Boltzmann simulations of blood flow non-Newtonian rheology and clotting processes," *Journal of Statistical Physics*, vol. 121, no. 1-2, pp. 209–221, 2005.

[47] C. H. Sun, R. K. Jain, and L. L. Munn, "Non-uniform plasma leakage affects local hematocrit and blood flow: implications for inflammation and tumor perfusion," *Annals of Biomedical Engineering*, vol. 35, no. 12, pp. 2121–2129, 2007.

[48] C. H. Sun and L. L. Munn, "Lattice-Boltzmann simulation of blood flow in digitized vessel networks," *Computers and Mathematics with Applications*, vol. 55, no. 7, pp. 1594–1600, 2008.

[49] M. M. Dupin, I. Halliday, C. M. Care, and L. L. Munn, "Lattice Boltzmann modelling of blood cell dynamics," *International Journal of Computational Fluid Dynamics*, vol. 22, no. 7, pp. 481–492, 2008.

[50] A. M. Artoli, A. G. Hoekstra, and P. M. A. Sloot, "Mesoscopic simulations of systolic flow in the human abdominal aorta," *Journal of Biomechanics*, vol. 39, no. 5, pp. 873–884, 2006.

[51] T. Hyakutake, T. Matsumoto, and S. Yanase, "Lattice Boltzmann simulation of blood cell behavior at microvascular bifurcations," *Mathematics and Computers in Simulation*, vol. 72, no. 2-6, pp. 134–140, 2006.

[52] L. Guigao and J. F. Zhang, "Boundary slip from the immersed boundary lattice Boltzmann models," *Physical Review E*, vol. 79, no. 2, article 026701, 2009.

[53] M. Tamagawa, K. Fukushima, and M. Hiramoto, "Prediction of thrombus formation in blood flow by CFD and its modeling," in *World Congress on Medical Physics and Biomedical Engineering 2006. IFMBE Proceedings*, vol. 14, pp. 3159-3160, Berlin, Heidelberg, 2007.

[54] A. B. Schelin, G. Karolyi, A. P. S. de Moura, N. A. Booth, and C. Grebogi, "Chaotic advection in blood flow," *Physical Review E*, vol. 80, no. 1, article 016213, 2009.

[55] L. L. Munn and M. M. Dupin, "Blood cell interactions and segregation in flow," *Annals of Biomedical Engineering*, vol. 36, no. 4, pp. 534–544, 2008.

[56] S. K. Doddi and P. Bagchi, "Three-dimensional computational modeling of multiple deformable cells flowing in microvessels," *Physical Review E*, vol. 79, no. 4, article 046318, 2009.

[57] B. Kaoui, G. Biros, and C. Misbah, "Why do red blood cells have asymmetric shapes even in a symmetric flow," *Physical Review Letters*, vol. 103, no. 18, article 188101, 2009.

[58] H. Noguchi, "Swinging and synchronized rotations of red blood cells in simple shear flow," *Physical Review E*, vol. 80, no. 2, article 021902, 2009.

[59] G. Yan, J. Zhang, Y. Liu, and Y. Dong, "A multi-energy-level lattice Boltzmann model for the compressible Navier–Stokes equations," *International Journal for Numerical Methods in Fluids*, vol. 559, pp. 41–56, 2007.

[60] X. W. Shan and H. D. Chen, "Lattice Boltzmann model for simulating flows with multiple phases and components," *Physical Review E*, vol. 47, no. 3, pp. 1815–1819, 1993.

[61] A. Ladd, "Numerical simulations of particulate suspensions via a discretized Boltzmann equation. Part 2. Numerical results," *Journal of Fluid Mechanics*, vol. 271, pp. 311–339, 1994.

[62] S. P. Dawson, S. Y. Chen, and G. D. Doolen, "Lattice Boltzmann computations for reaction–diffusion equations," *Journal of Chemical Physics*, vol. 98, no. 2, pp. 1514–1523, 1993.

[63] B. Ahrenholz, J. Tolke, and M. Krafczyk, "Lattice-Boltzmann simulations in reconstructed parametrized porous media,"

International Journal of Computational Fluid Dynamics, vol. 20, no. 6, pp. 369–377, 2006.

[64] H. J. Gao, J. Han, Y. Jin, and L. P. Wang, "Modelling micro-scale flow and colloid transport in saturated porous media," *International Journal of Computational Fluid Dynamics*, vol. 22, no. 7, pp. 493–505, 2008.

[65] G. W. Yan, "A lattice Boltzmann equation for waves," *Journal of Computational Physics*, vol. 161, pp. 61–69, 2000.

[66] Y. L. Duan and R. X. Liu, "Lattice Boltzmann model for two-dimensional unsteady Burgers' equation," *Journal of Computational and Applied Mathematics*, vol. 206, no. 1, pp. 432–439, 2007.

[67] G. W. Yan and J. Y. Zhang, "A higher-order moment method of the lattice Boltzmann model for the Korteweg–de Vries equation," *Mathematics and Computers in Simulation*, vol. 79, no. 5, pp. 1554–1565, 2009.

[68] S. Palpacelli and S. Succi, "Numerical validation of the quantum lattice Boltzmann scheme in two and three dimensions," *Physical Review E*, vol. 75, no. 6, article 066704, 2007.

[69] D. Alemani, F. Pappalardo, M. Pennisi, S. Motta, and V. Brusic, "Combining cellular automata and Lattice Boltzmann method to model multiscale avascular tumor growth coupled with nutrient diffusion and immune competition," *Journal of Immunological Methods*, vol. 376, no. 1-2, pp. 55–68, 2012.

[70] G. Pontrelli, I. Halliday, S. Melchionna, T. Spencer, and S. Succi, "Lattice Boltzmann method as a computational framework for multiscale haemodynamics," *Mathematical and Computer Modelling of Dynamical Systems*, vol. 20, no. 5, pp. 470–490, 2014.

[71] Y. Liu, "A lattice Boltzmann model for blood flows," *Applied Mathematical Modelling*, vol. 36, no. 7, pp. 2890–2899, 2012.

[72] S. Harrison, *The Use of the Lattice Boltzmann Method in Thrombosis Modelling, [Ph.D. Thesis]*, School of Medicine and Biomedical Sciences Academic Unit of Medical Physics, 2007.

[73] M. Neeman, H. Dafni, O. Bukhari, R. D. Braun, and M. W. Dewhirst, "In vivo BOLD contrast MRI mapping of subcutaneous vascular function and maturation: validation by intravital microscopy," *Magnetic Resonance in Medicine*, vol. 45, no. 5, pp. 887–898, 2001.

[74] F. Roudnicky, C. Poyet, P. Wild et al., "Endocan is upregulated on tumor vessels in invasive bladder cancer where it mediates VEGF-A–induced angiogenesis," *Cancer Research*, vol. 73, no. 3, pp. 1097–1106, 2013.

[75] Y. Wang, M. Nakayama, M. E. Pitulescu et al., "Ephrin-B2 controls VEGF-induced angiogenesis and lymphangiogenesis," *Nature*, vol. 465, no. 7297, pp. 483–486, 2010.

[76] F. J. H. Gijsen, F. N. Van de Vosse, and J. D. Janssen, "The influence of the non-Newtonian properties of blood on the flow in large arteries: steady flow in a carotid bifurcation model," *Journal of Biomechanics*, vol. 32, no. 6, pp. 601–608, 1999.

[77] R. J. Poole, M. P. Escudier, A. Afonso, and F. T. Pinho, "Laminar flow of a viscoelastic shear-thinning liquid over a backward-facing step preceded by a gradual contraction," *Physics of Fluids*, vol. 19, no. 9, article 093101, 2007.

[78] F. T. Pinho, P. J. Oliveira, and J. P. Miranda, "Pressure losses in the laminar flow of shear-thinning power-law fluids across a sudden axisymmetric expansion," *International Journal of Heat and Fluid Flow*, vol. 24, no. 5, pp. 747–761, 2003.

[79] M. P. Escudier and S. Smith, "Turbulent flow of Newtonian and shear-thinning liquids through a sudden axisymmetric expansion," *Experiments in Fluids*, vol. 27, no. 5, pp. 427–434, 1999.

[80] J. Tan, *Lattice Boltzmann Method and Its Applications in Soft Matter*, Lehigh University Publisher, 2015.

[81] S. Succi, *The Lattice Boltzmann Equation for Fluid Dynamics and Beyond*, Oxford University Press, Oxford, 2001.

[82] Y. Yan and J. Koplik, "Flow of power-law fluids in self-affine fracture channels," *Physical Review E*, vol. 77, no. 3, article 036315, 2008.